

Received xxx xx, xxxx, accepted xxx xx, xxxx, date of publication xxx xx, xxxx, date of current version xxx xx, xxxx.

Digital Object Identifier xxxx

# Photovoltaic Partial Shading Performance Evaluation with a DSTATCOM Controller

**BIBHUTI BHUSAN RATH<sup>1</sup>, MANOJ KUMAR PANDA<sup>1</sup>, (Senior Member, IEEE), BHOLA JHA<sup>1</sup>, AROBINDA DASH<sup>2</sup>, (Graduate Student Member, IEEE), SURYA PRAKASH<sup>2</sup>, (Graduate Student Member, IEEE), RANJAN KUMAR BEHERA<sup>2</sup>, (Senior Member, IEEE), KHALIFA AL HOSANI<sup>3</sup>, (Senior Member, IEEE), SRINIVASARAO TEGALA<sup>4</sup>, (Member, IEEE), and UTKAL RANJAN MUDULI<sup>3</sup>, (Member, IEEE)**

<sup>1</sup>Department of Electrical Engineering, Govind Ballabh Pant Institute of Engineering and Technology, Pauri Garhwal, Uttarakhand 246194, India (bibhutibhusanrath2007@gmail.com, pandamanoj123@rediffmail.com, bholajhaee@gmail.com).

<sup>2</sup>Department of Electrical Engineering, IIT Patna, Patna 801103, India (arobinda\_dash@yahoo.co.in, suryaprashele@gmail.com).

<sup>3</sup>Advanced Power and Energy Center, Department of Electrical Engineering and Computer Science, Khalifa University, PO Box 127788, Abu Dhabi, UAE (khalifa.halhosani@ku.ac.ae, utkal.muduli@ku.ac.ae).

<sup>4</sup>Department of Electrical and Electronics Engineering, Avanthi Institute of Engineering and Technology, Visakhapatnam, 531113, India (srinivasarao\_tegala@yahoo.co.in).

Corresponding author: Utkal Ranjan Muduli (utkal.muduli@ku.ac.ae).

This work was supported by the Ministry of Human Resource Development and Ministry of Power, Government of India, through IMPRINT under Project F. No. 1-18/2015-TS-TS.I; in part by the Khalifa University under Award KKJRC-2019-Trans2; and in part by the Advanced Technology Research Council ASPIRE Virtual Research Institute (VRI) Program, Abu Dhabi, United Arab Emirates, under Award VRI20-07.

**ABSTRACT** A solar photovoltaic distribution static compensator (SPV-DSTATCOM) under partial shading condition (PSC) is studied using a single-stage, 3-phase grid-connected mode. Under PSC, the performance of the grid-connected SPV-DSTATCOM is studied and addressed the issues such as active current sharing, reactive power control, and harmonic elimination. Rejection of DC offset with such PSC condition is an issue when using a conventional Proportional Resonant (PR) controller. As a result of this research, a new and improved PR (IPR) based second-order generalized integrator (SOGI) has been developed that has unity gain at the fundamental frequency and greater DC offset rejection capability to address the PR controller shortcomings. The proposed controller's performance is evaluated in both steady-state and dynamic conditions with varying loads and different PSC conditions. An experimental evaluation of the proposed controller's design assumptions is also presented in the form of a comparison with both the PR controller and the adaptive PR controller.

**INDEX TERMS** Reactive Power Supply, Partial Shading Condition, Proportional Resonant Controller, Power System Harmonics, Second-Order Generalized Integrator.

## I. INTRODUCTION

In the last few years, increasing focus has been given towards Renewable Energy (RE) generation because of the perishable nature of fossil fuels, growth in emission rates along with the major issue of global warming. Introduction of RE sources is capable of immediately satisfying the growing demand of energy [1]. Decentralized energy generation through RE sources possesses several distinct attributes compared to the traditional sources of energy production. Hence, multidisciplinary research activities have been taking place to enhance the available power conversion techniques along with the

introduction of brand-new techniques regarding novel configuration, topologies and control mechanisms. Considerable importance is given towards the extensive utilization of solar photovoltaic cells regarding grid-tied situations because of the adverse effects of green house gas, global warming, and security along with the payback period [2].

Making use of solar photovoltaic systems (SPV) largely relies upon the fluctuation in the solar radiation along with the intensity of disturbances occurring in the grid. In case of a particular grid initialization, large amounts of photovoltaic panels are attached to the power grid. Concerning these

systems, Partial Shading Condition (PSC) arises because of the shadow of either trees or buildings or due to moving clouds. At such situation, the power vs voltage curve seems more complex because of the emergence of numerous local maximum power points (MPPs). Out of these local maximum power points, one and only peak illustrates the global MPP (GMPP). Traditional methods become inefficient in accurately tracking GMPP as well as can be erroneous in tracking any local MPP, which results in a sizable deduction in the production of energy as well as efficiency. New research articles demonstrate the significance of tracking GMPP in case of quickly changing irradiance scenarios [3]–[5]. Hence, the most significance feature of grid-connected photovoltaic system is generating the optimum amount of power in accordance with changing solar radiation. One of the most important aspects for researchers is determining the global maximum under partial shading conditions. Some recent studies include bidirectional DPP fly back converters [6], Levy flight (JAYA-LF) based JAYA algorithm [7], flying squirrel search optimization (FSSO) [8], a spline-MPPT Technique [9], PSO based method [10]. These methodologies have trade-offs between fast tracking and accuracy of GMPP. One of the most advanced methodologies called Extreme Seeking Algorithm (ESA) [11] is employed in this paper for its better performance while tracking the GMPP.

Concerning a grid-tied PV system, a small amount of fluctuation in the voltage of the inverter output as well as the grid voltage at the point of common coupling (PCC) can result in a much larger amount of inrush current within the system. Hence, a customized control mechanism is needed in case of grid synchronization. PLL is highly recommended by researchers to fulfil the above requirements [12]. Moreover, the phase-locked loop is also entitled to several limitations like the nonlinear property, complex tuning system, and slack as well as diminishing outcomes in case of fragile grid conditions [13], [14]. To address these drawbacks, various modern innovative tuning mechanisms are suggested in article [15]–[17]. The above-mentioned innovative tuning models compete with computational burden, system stability, system's dynamic response, enhanced system performance like sharing of active current in case of the existence of two different resources, issues regarding the quality of power, compensation of reactive power, harmonic elimination, improvement of grid current as well as grid voltage in terms of Total Harmonic Distortion (THD). However, these advanced tuning mechanisms again result in complex control measures and minimizing the system's dynamic performance.

The prime objective of grid-integrated SPV-DSTATCOM is to feed active as well as reactive power within the system in the presence of solar radiation [18], [19]. Apart from that, without solar radiation, this injects the harmonic compensation power needed by the load named as DSTATCOM. It becomes very much essential in keeping the grid current harmonic free, sinusoidal, steady as well as unity power factor operation utilizing voltage control. Current regulation action is carried out via the hysteresis current regulator, linear

PI regulator, or predictive regulator. Such type of regulator is again classified to a synchronous rotating  $dq$  frame as well as a stationary reference frame. However, the 3-phase synchronous reference frame regulator yields undesirable results, since this requires data on the phase angle with respect to the rotating frame. The regulator performs erroneously when the evaluation of phase angle becomes inaccurate. However, during the same time period, a stationary frame regulator outcome known as proportional resonance (PR) controller yields desirable results [20]. PR controller is used in the case of active power filter, PV systems, wind turbines, control rectifiers, Induction Motor (IM) drives as well as for fuel cell operations [21]–[26]. Merits of PR controller involve 1) swift dynamic response accompanied by zero steady state fault, 2) relatively less computational load since this does not need data on  $\alpha\beta$  frame, 3) free from phase locked loop. However, it needs an appropriate synchronization technique with respect to grid-connected implementations [27], [28]. Deriving a high gain at resonance frequency is one of the major demerit points of the PR controller. The undesirable peak leads to faulty evaluation with respect to the usual PR controller. As a consequence, this results in a sizable loss of performance. In addition to that, the existence of 2 unifiers/harmonizers is accountable for the fluctuation of the voltage frequency during the time where the unbounded gain is obtained taking into account the anticipated resonant frequency because of the dislocation of the resonant pole. It is demonstrated in terms of a significant steady state fault [29]. An APR regulator is introduced for addressing this issue of steady state error [30]. This proposes a fourth-order band pass filter along with an adaptive integration technique for tracking the deviation in grid frequency. As a result, this minimizes the frequency sensitivity. However, this creates more complications as well as puts more computational load on the system. As a consequence, the measured frequency becomes inaccurate because of the existence of DC offset. It leads to the superimposition of the low frequency component on the basis of the mean value of the calculated frequency. Existence of DC offsets gives rise to both fundamental frequency variations and DC injection through grid-connected converters. Eliminating such variations becomes burdensome because of its low-frequency characteristic [31]. Hence, the international standard IEC 61727 has proposed a check upon the limits of DC offset in case of grid-connected PV s under 1% of its rated output current [32]. Such limitations reveal the significance of the declining of DC offset prevailing within the input signal of the regulator.

The following points summarize the contributions of this paper.

- An advanced PR controller built upon the SOGI (IPR-SOGI) is proposed for addressing the issues concerning both high gains with phase jump and DC offsets present in the input signal.
- A method to generate a positive sequence input signal is adopted in the proposed controller using the proposed

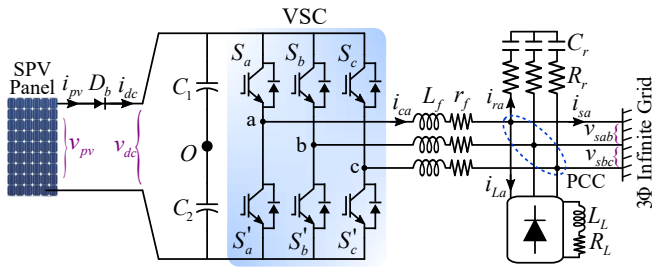


FIGURE 1. Configuration of grid integrated SPV-DSTATCOM.

IPR-SOGI. This can be further utilized for unit template generation and sequence load current extraction.

- The proposed controller is simple to implement with lower computational burden with better dynamic response compared to various complex algorithms. It has greater DC offset rejection capability, the greater harmonic reduction potential meanwhile increases the stability of the system.
- The performance of the proposed controller is confirmed under partial shading conditions accompanied by several distinct loading scenarios alongside dynamic conditions.
- Excellent results are obtained through a comparison of the experimental performance of the conventional PR controller with the proposed IPR-SOGI based controller.

The following five sections make up this document: the system topology and the control architecture of the improved PR controller are described in Section II, and the experimental validation and results with other control structures are discussed in Section III of the article. Section IV extends the conclusion.

## II. PROPOSED IPR-SOGI METHOD FOR DSTATCOM CONTROL

### A. SYSTEM DESCRIPTION

Devices such as static synchronous compensator (STATCOM) are used to regulate alternating current energy transmission networks, such as the North American Electric Reliability Corporation (NERC). Using an electronic voltage-source converter (VSC), it can provide or sink reactive alternating current (AC) power from a grid. As a fast-compensating reactive power source, distributed STATCOM (DSTATCOM) reduces voltage changes like sags, surges, and flicker produced by quickly changing reactive power demand on the transmission or distribution system [33]. Because a DC capacitor at DC-side of VSC is used to maintain the DC-link voltage constant, a DSTATCOM has a low active power generation capacity. A suitable energy storage device can be connected across the DC capacitor to boost its active power capability. Hence, a solar photovoltaic array is connected at DC-side of DSTATCOM to produce an SPV-DSTATCOM structure, as illustrated in Fig. 1. Now, the SPV-DSTATCOM has the capability to supply both active and reactive power to

the utility grid with higher reliability. The amount of active power generated depends on the solar irradiance and the panel temperature, wherever the reactive power generation completely depends on the amplitude of the grid voltage. This is because the reactive power demand by load connected at the point of common coupling (PCC) regulates the grid voltage. The more inductive the load is, reactive power demand at the PCC point will be more, which decreases the grid voltage at the PCC point. If the DC link capacitor will be utilized for such compensation, it can support reactive power for a period of few (2 to 3) cycles. More the DC-link capacitance, more duration (only for transient period) for which the DC-link capacitor can release the stored energy in the form of reactive power to the grid. As the voltage level of DC-link is supported by the PV system, it is most likely that the DC-link can support the reactive power to the local load at PCC to stabilize the PCC voltage to some extent (until the rated value of the PV VSC system). SPV-DSTATCOM generates appropriate compensating reactive current through the line filter during injection or absorption of reactive power. The DSTATCOM can deliver reactive power when the AC side voltage ( $v_i$ ) of VSC is greater than the PCC voltage ( $v_s$ ); on the other hand, DSTATCOM absorbs reactive power when  $v_s$  is greater than  $v_i$ . Irrespective of the reactive current direction, VSC operates in buck mode and the DC-link voltage ( $v_{dc}$ ) should be always greater than the peak of the line-to-line AC side voltage of the inverter. The line filter between the VSC and PCC, as shown in Figure 1, plays an important role here for the reactive power transfer. The line filter ( $L_f$  with parasitic resistance  $r_f$ ) at PCC is also used for filtering out high-frequency ripples in the phase current. The line filter inductance can be calculated as per the relation (1).

$$L_f = \frac{(v_i - v_g)v_g}{2v_i f_{sw}(HB)} \quad (1)$$

where HB is the selected hysteresis band and  $f_{sw}$  is the switching frequency of VSC. Again, the ripple filter (i.e., series connected resistor,  $R_r$  and a capacitor  $C_r$ ) is used to eliminate noise from the voltage signals. The ripple filter is so designed that it offers very high impedance at the fundamental frequency and it offers low impedance to the switching frequency component. In order to satisfy this condition,  $R_r C_r \ll T_s$  holds good. Considering  $R_r C_r = T_s/4$  at switching frequency of  $f_{sw} = 10kHz$  ( $1/T_s$ ), the value of capacitor is calculated as  $C_r = 4.2\mu F \approx 10\mu F$  (as per availability) with  $R_r = 6\Omega$ . To analysis the SPV-DSTATCOM behavior at PCC, three-phase alternating current main is connected to the three-phase nonlinear load. The nonlinear load is created by combining an unregulated diode bridge rectifier with a series of R-L loads. The voltage and current sensors are used to measure the PCC line-to-line voltage, photovoltaic voltage and current, load, and grid side phase currents.

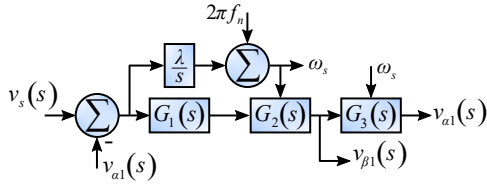


FIGURE 2. Block diagram of IPR-SOGI with original and quadrature generation

**B. PROPOSED IPR-SOGI**

Considering the sinusoidal input signal  $v_s = V_{sm} \sin(\omega_s t + \phi_v)$ , the magnitude step response of an ideal generalized integrator (GI) can be represented as (2). Here,  $V_{sm}$ ,  $\omega_s$  and  $\phi_v$  are the maximum amplitude, angular frequency, and phase angle of the input signal, respectively.

$$v_{\alpha 1} = V_{sm} (1 - e^{-k_{\alpha} t}) \sin(\omega_s t + \phi_v) \quad (2)$$

where  $v_{\alpha 1}$  and  $v_{\beta 1}$  are the closed-loop response of GI and its quadrature component, respectively.  $k_{\alpha}$  is a gain that depends upon the settling time of the step response of GI. In Laplace domain,  $v_s \rightarrow v_s(s)$  and  $v_{\alpha 1} \rightarrow v_{\alpha 1}(s)$  can be denoted as (3).

$$v_s(s) = \frac{V_{sm} \omega_s \cos \phi_v}{s^2 + \omega_s^2} + \frac{V_{sm} s \sin \phi_v}{s^2 + \omega_s^2}$$

$$v_{\alpha 1}(s) = \frac{V_{sm} \omega_s \cos \phi_v}{s^2 + \omega_s^2} + \frac{V_{sm} s \sin \phi_v}{s^2 + \omega_s^2} - \frac{V_{sm} k_{\alpha} (\cos \phi_v + \sin \phi_v) + V_{sm} s \sin \phi_v}{(s + k_{\alpha})^2 + \omega_s^2} \quad (3)$$

Now, the open-loop transfer function of the GI with unit feedback can be obtained as (4).

$$G(s) = \frac{k_{\alpha} s}{s^2 + \omega_s^2} + \frac{k_{\alpha} \omega_s}{s^2 + \omega_s^2} \left( \frac{-\omega_s \sin \phi_v + (s + k_{\alpha}) \cos \phi_v}{\omega_s \cos \phi_v + (s + k_{\alpha}) \sin \phi_v} \right) \quad (4)$$

The open-loop transfer function in (4) contains a second-order denominator; hence, GI is further considered as second-order GI (SOGI). In practical conditions, it is difficult to distinguish the initial phase of the input signal  $v_s$ ; thus  $\phi_v$  is considered as zero. Now, the expression for open-loop transfer function of SOGI ( $G(s)$ ) can be reconfigured as (5).

$$G(s) = \frac{2k_{\alpha} s + k_{\alpha}^2}{s^2 + \omega_s^2} = \underbrace{\left(1 + \frac{k_{\alpha}}{2s}\right)}_{G_1(s)} \underbrace{\left(\frac{2k_{\alpha}}{\omega_s}\right)}_{G_2(s)} \underbrace{\left(\frac{\omega_s/s}{1 + (\omega_s/s)^2}\right)}_{G_3(s)} \quad (5)$$

where  $G_1(s)$ ,  $G_2(s)$  and  $G_3(s)$  are sub transfer functions of  $G(s)$ . The transfer function  $G(s)$  with the unit feedback provides the closed transfer function as mentioned in (6).

$$G_{\alpha 1}(s) = \frac{G(s)}{1 + G(s)} \quad (6)$$

With the grid voltage signal as input to  $G_{\alpha 1}(s)$ , variations in the impedance of the system leads to the possibility of resonance, resulting in a competent reliability of the controller. To avoid such a scenario, another PR term needs to be added

in  $G(s)$ . This modification can be achieved by changing the loop gain of  $G_3(s)$  in its feedback path. Let  $H_{\beta}(s)$  be the feedback path in  $G_3(s)$  and can be denoted as (7).

$$H_{\beta}(s) = 1 + \frac{\omega_s}{s} + k_{\beta} \left(1 + \left(\frac{\omega_s}{s}\right)^2\right) \quad (7)$$

where  $k_{\beta}$  is introduced as an additional gain in the feedback path. Now,  $G_3(s)$  can be modified as (8).

$$G_3(s) = \frac{\omega_s/s}{1 + (\omega_s/s) H_{\beta}(s)} \quad (8)$$

Considering  $G_3(s)$  in (5), the overall transfer function  $G_{\alpha 1}(s)$  and  $G_{\beta 1}(s)$  of proposed IPR-SOGI can be derived as (9)-(10), respectively.

$$G_{\alpha 1}(s) = \frac{v_{\alpha 1}(s)}{v_s(s)} = \frac{2k_{\alpha} s^2 + k_{\alpha}^2 s}{s^3 + (2k_{\alpha} + k_{\beta} \omega_s + \omega_s) s^2 + (\omega_s^2 + k_{\alpha}^2) s + k_{\beta} \omega_s^3} \quad (9)$$

$$G_{\beta 1}(s) = \frac{v_{\beta 1}(s)}{v_s(s)} = \frac{2k_{\alpha} \omega_s s + k_{\alpha}^2 \omega_s}{s^3 + (2k_{\alpha} + k_{\beta} \omega_s + \omega_s) s^2 + (\omega_s^2 + k_{\alpha}^2) s + k_{\beta} \omega_s^3} \quad (10)$$

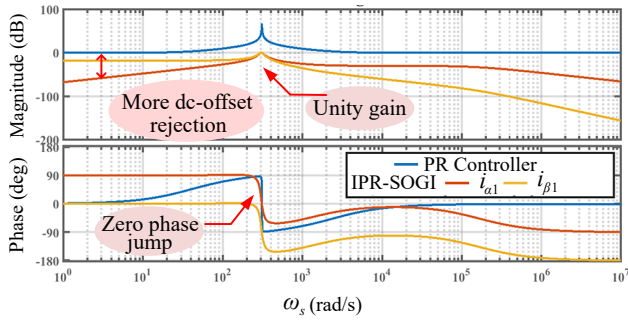
Fig. 2 show the block diagram for generating  $v_{\alpha 1}(s)$  and  $v_{\beta 1}(s)$ , respectively, from  $v_s(s)$ . Here, the deviation in grid angular frequency ( $2\pi \Delta f_s$ ) can be calculated by integrating the error generated from  $v_s(s) - v_{\alpha 1}(s)$  with a gain  $\lambda$ .  $\omega_s$  can be generated further by adding  $2\pi \Delta f_s$  with the nominal grid angular frequency ( $2\pi f_n$ ). The estimated value of  $\omega_s$  is utilized to evaluate the transfer functions  $G_2(s)$  and  $G_3(s)$ . As a modified PR controller is utilized in the SOGI, this concept is further classified as IPR-SOGI. IPR-SOGI Is capable of generating the original signal with its quadrature component with better dynamics and completely dependent on the selection of the gains  $k_{\alpha}$  and  $k_{\beta}$ . The optimum selection of these gains is possible through the bode and root locus representation of the transfer function  $G_{\alpha 1}(s)$  and  $G_{\beta 1}(s)$ , which is illustrated in Fig. 3(a) and 3(b), respectively. It can be observed that the phase margin and gain margin are both positive, indicating that the system is running smoothly when  $k_{\alpha}=2500$  and  $k_{\beta}=500$ . It is also possible to design the parameters  $k_{\alpha}$  and  $k_{\beta}$  from the time domain analysis as per the following procedure.

- Step 1: Select the settling time  $t_s$  for the IPR-SOGI controller.
- Step 2: Set damping ratio  $\zeta$  to 0.707 for low overshoot and less settling time.
- Step 3: Determine the natural oscillation angular frequency  $\omega_n$  as (11).

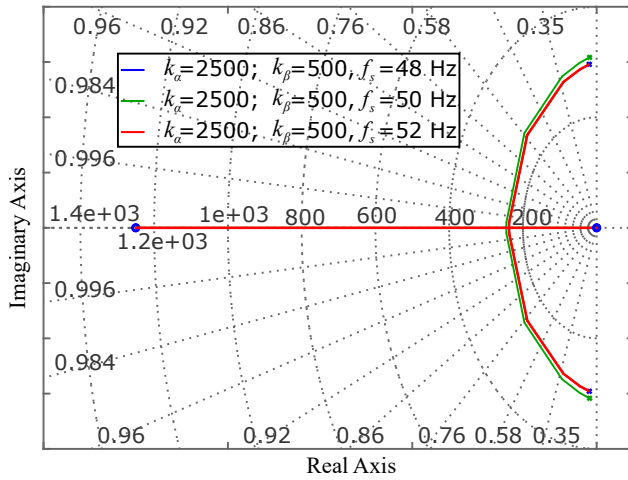
$$\omega_n = \frac{4.4}{\zeta t_s} \quad (11)$$

- Step 4: Consider the characteristic equation as  $1 + G(s) = (s+c)(s+2\zeta\omega_n s + \omega_n^2)$ , where the variable c should satisfy  $c > G_d \zeta \omega_n$  with  $G_d > 5$  for optimum transient response. Now, the controller gains  $k_{\alpha}$  and





(a) Comparative study of IPR-SOGI with conventional PR based SOGI



(b) Root locus analysis with system frequency variation

FIGURE 3. Stability analysis through root locus and frequency response.

$k_\beta$  can be obtained as (12).

$$k_\beta = \frac{G_d \zeta \omega_n^3}{\omega_s^3} \quad (12)$$

$$k_\alpha = \frac{1}{2} ((1 + G_d) \zeta \omega_n - \omega_s (1 + k_\beta))$$

When compared to the proportional resonant (PR) controller, the analysis corresponding to the proposed IPR-SOGI revealed that the suggested controller performs as a band pass filter and has better DC-offset discarding ability. However, the PR controller acts as a notch filter and has a flat characteristic on the magnitude plot. Furthermore, when compared to a traditional PR controller, this suggested IPR-SOGI controller produces zero phase jump. The robustness of this proposed controller interacts negatively with the fluctuation in grid frequency in transitory scenarios, as illustrated in Fig. 3(b).

### C. MPPT CONTROL ALGORITHM

An improved ESA has been implemented to track the GMPP from the non-linear characteristics PV curve, as shown in Fig. 4. It is efficient under fast and persistent changes in solar irradiance, overcoming disturbances and uncertainties. The perturbed power and perturbed current contains significant ripples. In order to filter out these ripple, two High Pass Filters (HPF) having cut-off frequency 100 Hz are introduced.

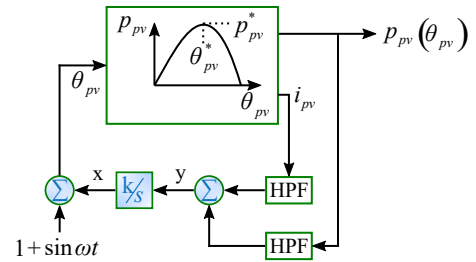


FIGURE 4. Block diagram of improved ESA algorithm

The outputs of these HPF are added together and is termed as demodulated signal ( $y$ ). The demodulated signal is integrated and multiplied with a small value of  $k = 0.2$  to generate the adaptive signal ( $x$ ). Here, a perturbation signal ( $1 + \sin \omega t$ ) is added to the input adaptive signal ( $x$ ), which results in the maximum output power and can track the GMPP adaptively. Moreover, the improved ESA is an adaptive controller and does not require fine-tuning for better performance.

### D. SPV-DSTATCOM CONTROL ARCHITECTURE

The SPV-DSTATCOM control architecture includes the extraction of the positive sequence voltage as well as their quadrature elements via the IPR-SOGI control mechanism. Furthermore, such elements are used for evaluating unit templates for grid synchronization. This proposed control framework is then used to evaluate the load current fundamental components that are used for measuring the reference current with respect to the hysteresis current controller for generating gate pulses for grid-tied inverter.

#### 1) Unit template generation

Initially, two voltage sensors are used at PCC to measure the line voltage between phases a-b ( $v_{sab}$ ) and phases b-c ( $v_{sbc}$ ). The phase voltages at PCC are then estimated using (13).

$$v_{sa} = \frac{2v_{sab} + v_{sbc}}{3}$$

$$v_{sb} = \frac{-v_{sab} + v_{sbc}}{3} \quad (13)$$

$$v_{sc} = \frac{-v_{sab} - 2v_{sbc}}{3}$$

Following that,  $abc$ -frame PCC phase voltages ( $v_{sa}, v_{sb}, v_{sc}$ ) can be transformed to the stationary  $\alpha\beta$ -frame ( $v_{s\alpha\beta}$ ) using (14) to carry out IPR-SOGI.

$$v_{s\alpha\beta} = \frac{2}{3} \begin{bmatrix} 1 & a & a^2 \end{bmatrix} \begin{bmatrix} v_{sa} & v_{sb} & v_{sc} \end{bmatrix}^T \quad (14)$$

Here,  $v_{s\alpha} = \Re(v_{s\alpha\beta})$  and  $v_{s\beta} = \Im(v_{s\alpha\beta})$  are representing the voltage in  $\alpha$ -axis and  $\beta$ -axis, respectively.  $v_{s\alpha}$  ( $v_{s\beta}$ ) is given as input to the IPR-SOGI, while  $v_{\alpha 1}$  and  $v_{\beta 1}$  ( $v_{\alpha 2}$  and  $v_{\beta 2}$ ) are taken as output from the IPR-SOGI. The flow diagram of the corresponding conversion procedure is depicted in Fig. 5. The estimation of the positive sequence voltage in  $\alpha\beta$ -frame from these output quantities are computed as per

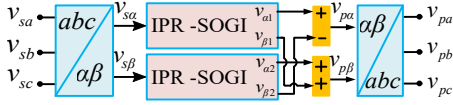


FIGURE 5. Positive sequence generator using IPR-SOGI.

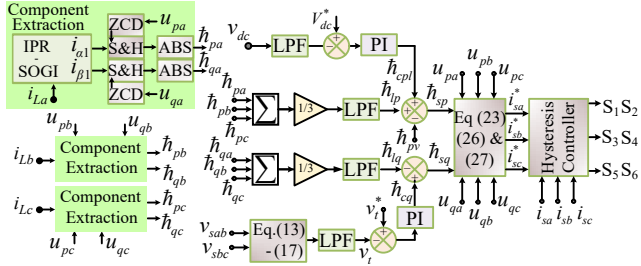


FIGURE 6. SPV-DSTATCOM overall control structure for switching pulse generation.

$$(15) \quad v_{p\alpha} = v_{\alpha 1} - v_{\beta 2} \quad v_{p\beta} = v_{\alpha 2} + v_{\beta 1} \quad (15)$$

Using  $\alpha\beta$ -to- $abc$  frame conversion, the positive sequence voltage in  $abc$ -frame ( $v_{pa}, v_{pb}, v_{pc}$ ) can be computed as using (16).

$$\begin{bmatrix} v_{pa} \\ v_{pb} \\ v_{pc} \end{bmatrix} = \begin{bmatrix} 1 & 0 \\ \cos(2\pi/3) & \sin(2\pi/3) \\ \cos(4\pi/3) & \sin(4\pi/3) \end{bmatrix} \begin{bmatrix} v_{p\alpha} \\ v_{p\beta} \end{bmatrix} \quad (16)$$

Furthermore, the three-phase unit template ( $u_{pa}, u_{pb}, u_{pc}$ ) can be derived as (17) from the positive sequence phase voltage.

$$u_{pa} = v_{pa} \frac{1}{v_t} \quad u_{pb} = v_{pb} \frac{1}{v_t} \quad u_{pc} = v_{pc} \frac{1}{v_t} \quad (17)$$

where  $v_t = \sqrt{\frac{2}{3} (u_{pa}^2 + u_{pb}^2 + u_{pc}^2)}$  represent the amplitude of the terminal voltage. Equation (17) can also be used to estimate the quadrature unit template ( $u_{qa}, u_{qb}, u_{qc}$ ) in (18).

$$\begin{aligned} u_{qa} &= 0.577(u_{pc} - u_{pb}) \\ u_{qb} &= 0.288(3u_{pa} + u_{pb} - u_{pc}) \\ u_{qc} &= 0.288(-3u_{pa} + u_{pb} - u_{pc}) \end{aligned} \quad (18)$$

These measured positive sequence unit templates in conjunction with the quadrature unit templates are used to generate the fundamental positive sequence as well as the quadrature element of the load current, as discussed in the following section.

## 2) Load current component extraction

The estimated 3-phase load current consists of a fundamental component, a harmonic component, and a quadrature component. The fundamental component represents the active power, whereas the quadrature component represents the reactive power. First, the fundamental positive sequence components of the load current of the corresponding phases are measured using the procedure shown in Fig. 5. Furthermore,

the fundamental elements of load current are utilized to measure the reference currents in relation to SPV-DSTATCOM. Fig. 6 depicts the process of fundamental component estimation process through the proposed IPR-SOGI algorithm. These measured fundamental components are passed through the sample, followed by a hold circuit and zero-crossing detector (ZCD). Within each phase, two distinct ZCDs are used to generate  $\hat{h}_{px}$  or  $\hat{h}_{qx}$ ,  $x \in \{a, b, c\}$ . The unit template, i.e.,  $u_{px}$  ( $u_{qx}$ ) is used to activate the ZCD with respect to  $\hat{h}_{px}$  ( $\hat{h}_{qx}$ ). In this case, equation (19) calculate the mean value of direct ( $\hat{h}_{lp}$ ) and quadrature ( $\hat{h}_{lq}$ ) components, respectively.

$$\hat{h}_{lpa} = \frac{1}{3} \sum_x \hat{h}_{px} \quad \text{and} \quad \hat{h}_{lqa} = \frac{1}{3} \sum_x \hat{h}_{qx} \quad (19)$$

## 3) Loss Term Estimation

Surplus current is extracted from the grid to keep the actual DC-link capacitor voltage ( $v_{dc}$ ) within its reference value ( $V_{dc}^*$ ) when operating the SPV-DSTATCOM. This maintains the DC-link voltage at its reference voltage during the transitory periods of charging and discharging. Surplus currents, on the other hand, are usually in phase with the grid voltage, resulting in additional losses if the system is operated. The difference between the reference DC-link voltage and the actual DC-link voltage is regarded as the DC-link voltage error and is catered for within the proportional integral (PI) controller to calculate the current with regard to the additional power losses. In this case, equation (20) represents the discrete-time implementation of the PI controller to determine the loss component  $\hat{h}_{cpl}^{(k)}$ .

$$\hat{h}_{cpl}^{(k)} = \hat{h}_{cpl}^{(k-1)} + k_{p1}[v_{err}^{(k)} - v_{err}^{(k-1)}] + k_{i1}v_{err}^{(k)} \quad (20)$$

where  $k_{p1}$  and  $k_{i1}$  represent the PI gains and are tabulated in Table I.  $k$  denotes the present sample of the controller. The DC-link error voltage is represented by  $v_{err}^{(k)} = V_{dc}^* - v_{dc}^{(k)}$  with  $V_{dc}^*$  calculated from the GMPP of ESA algorithm.

## 4) Reference current formation

For the reference current generation, the current component corresponding to active and reactive power generation along with the loss components need to be estimated and summed up as per Fig. 6. PV current ( $i_{pv}$ ) and PV voltage ( $v_{pv}$ ) are initially measured through suitable sensors and supplied to MPPT mentioned in [11]. By utilizing the ESA MPPT algorithm,  $V_{dc}^*$  is generated through the appropriate selection of step size. The supplied current from PV can be estimated from the PV power ( $p_{pv} = i_{pv}v_{pv}$ ) and the terminal voltage  $v_t$  as mentioned in (21).

$$\hat{h}_{pv} = \frac{2}{3} \frac{i_{pv}v_{pv}}{v_t} \quad (21)$$

The effective component of load current  $\hat{h}_{sp}$  is calculated from the loss component as well as the average load active component provided by the grid and can be estimated by (22).

$$\hat{h}_{sp} = \hat{h}_{lpa} + \hat{h}_{cpl} - \hat{h}_{pv} \quad (22)$$

Fundamental reference currents are obtained by multiplying the subsequent component by its respective unit template, which is represented in (23).

$$i_{pa}^* = \hat{h}_{sp} U_{pa} \quad i_{pb}^* = \hat{h}_{sp} U_{pb} \quad i_{pc}^* = \hat{h}_{sp} U_{pc} \quad (23)$$

Similarly, the quadrature component of the load current is obtained by measuring  $\hat{h}_{sq}$ , i.e., the reactive weight component. The corresponding reactive weight component is calculated by subtracting the fundamental component's average reactive weight from the AC component's estimated reactive weight by (24).

$$\hat{h}_{sq} = \hat{h}_{cq} - \hat{h}_{lqa} \quad (24)$$

Concerning ZVR, the reactive reference current is obtained from the voltage control loop in addition to the proportional integral controller output, as shown in (25).

$$\hat{h}_{cq}^{(k)} = \hat{h}_{cq}^{(k-1)} + k_{p2}[v_{t,err}^{(k)} - v_{t,err}^{(k-1)}] + k_{i2}v_{t,err}^{(k)} \quad (25)$$

where  $v_{t,err}(i) = v_t^*(i) - v_t(i)$  represents the terminal voltage error.  $v_t^*(i)$  is the reference terminal voltage.  $k_{p2}$  and  $k_{i2}$  symbolize the PI gains and are tabulated in Table 1. Equation (26) is used to calculate the reactive weight component in relation to the load current.

$$i_{qa}^* = U_{qa} \hat{h}_{sq} \quad i_{qb}^* = U_{qb} \hat{h}_{sq} \quad i_{qc}^* = U_{qc} \hat{h}_{sq} \quad (26)$$

Finally, equation (27) calculated the reference grid current in relation to the hysteresis current controller.

$$i_{sa}^* = i_{pa}^* + i_{qa}^* \quad i_{sb}^* = i_{pb}^* + i_{qb}^* \quad i_{sc}^* = i_{pc}^* + i_{qc}^* \quad (27)$$

The reference current error can be generated here by the deduction of sensed grid currents ( $i_{sa}, i_{sb}, i_{sc}$ ) from the grid reference currents ( $i_{sa}^*, i_{sb}^*, i_{sc}^*$ ). Such errors are committed using a hysteresis current controller (HCC) to generate gate pulses that power the grid-connected inverter. The switching frequency ( $f_{sw}$ ) of the VSC is regulated by the hysteresis band (HB) of HCC. To ensure that the resonant frequency ( $f_{res}$ ) is unaffected by the minimum switching frequency ( $f_{sw,min}$ ), the frequency band is selected so that the maximum switching frequency ( $f_{sw,max}$ ) does not exceed the calculated switching frequency limits of the Insulated-gate bipolar transistor (IGBT) switch [34]. VSC and filter design can be readily performed by establishing a switching frequency band as (28) [35].

$$10f_s < f_{res} < f_{sw,min} < f_{sw,avg} < f_{sw,max} \quad (28)$$

where  $f_s$  represent the grid frequency. The maximum switching frequency, DC-link voltage, and grid voltage at PCC must all be taken into account when determining the appropriate current hysteresis band for a three-phase VSC. In other words, HB need not be extremely small or incredibly large in any way. The HCC tracking capability is additionally enhanced by the trade-off between permissible injected PCC current % THD (within the IEEE-519 limit of 5%) and average switching frequency ( $f_{sw,avg}$ ). Consider  $I_i$  be the

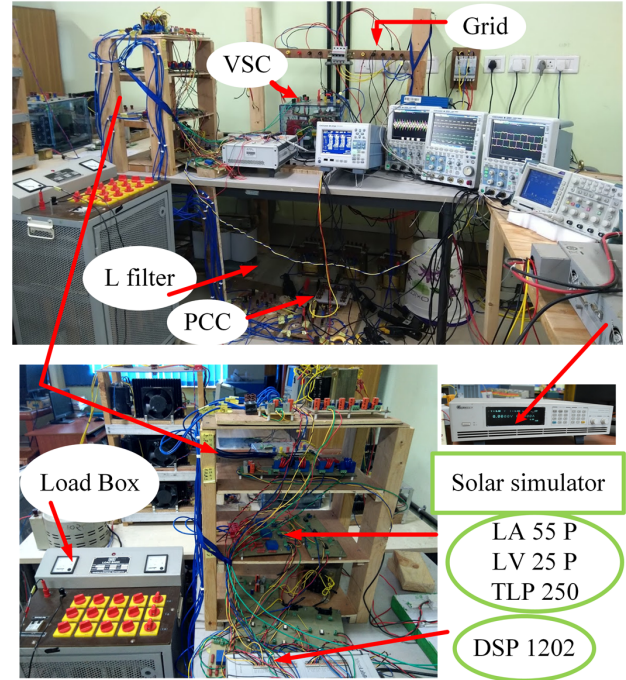


FIGURE 7. Experiment set-up developed at laboratory.

TABLE 1. Experimental set-up parameters

System quantities	Values
Source voltage (rms)	60 V, 60 V, 60 V L-N, 50 Hz
Feeder impedance	$R_s = 0.3 \Omega$ , $L_s = 0.03 \text{ mH}$ , $R_s / X_s = 3.185$
Ripple filter	$R_r = 6 \Omega$ , $C_r = 10 \mu\text{F}$
nonlinear load	3- $\Phi$ rectifier with RL load of 4 $\Omega$ , 40 mH
Load power	$P_L = 565\text{W}$
Load current	7.4 A
PI tuning parameter	$k_{p1} = 0.152$ , $k_{i1} = 0.016$ , $k_{p2} = 0.0136$ , $k_{i2} = 0.0019$
DSTATCOM parameter	$V_{dc}^* = 107 \text{ V}$ , $C_{dc} = 2200 \mu\text{F}$ , $L_f = 5 \text{ mH}$
PV emulator rating	$P_{mpp} = 1600 \text{ W}$ , $V_{GMPP} = 106.4 \text{ V}$ , $I_{GMPP} = 15.029 \text{ A}$ , $V_{oc} = 125.2 \text{ V}$ , $I_{sc} = 16.268 \text{ A}$

rated value of the injected current. A fixed-band hysteresis current regulation limit of between 5% of  $I_i$  ( $0.05I_i$  A) in the inverter side current ripple is considered acceptable.

### III. EXPERIMENTAL VERIFICATION

In the laboratory, an experimental test bench of grid-integrated SPV-DSTATCOM is designed and illustrated in Fig. 7. This test bench is used to validate the performance of the suggested control methodology and includes a solar photovoltaic emulator (Chroma 62020H-150S), a 3-phase 2-level VSC (using 6 SEMIKRON SKM100GB063D IGBT



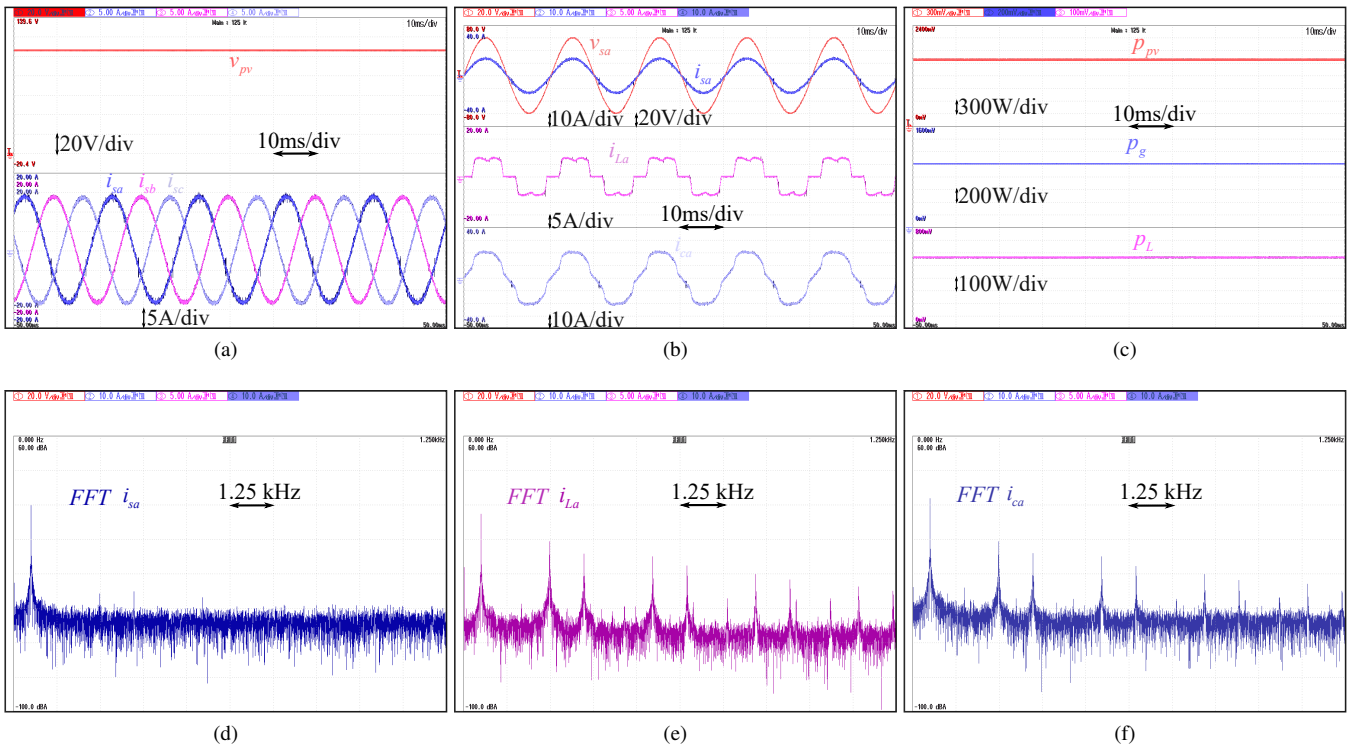


**FIGURE 8.** Experimental verification of Grid tied SPV system with PSC under balance grid and balance non-linear loading: (a)  $v_{pv}, i_{sa}, i_{sb}, i_{sc}$  (b)  $v_{sa}, i_{sa}, i_{ca}, i_{La}$  (c)  $p_{pv}, p_g, p_L$  (d) THD of  $i_{sa}$  (e) THD of  $i_{La}$ , (f) THD of  $i_{ca}$ .

switches), interfacing inductors, a ripple filter, a 3-phase diode bridge rectifier, and a nonlinear R-L load. Table 1 show the experimental test parameters for the grid-connected SPV-DSTATCOM system. The voltage transducers (LEM LV 25P) and current transducers (LEM 55P) are used to measure the line voltage and current signals. The steady and transient state waveforms are recorded using a 4-channel YOKOGAWA WT500 power analyzer and a 4-channel YOKOGAWA DSO DCM2024 digital storage oscilloscope. The control mechanism is implemented by utilizing the digital signal processor dSPACE MicroLabBox DS1202. The pulses generated by the DS1202 are directed through the TLP-250 driver circuit to the VSC switches. Considering computation time of the proposed controller, the sample time of the DS1202 is set to  $50 \mu s$ . At the time of the experiment, the DC-link voltage follows the SPV voltage through GMPP algorithm and  $V_{mpp}$  is maintained at 106.4 V for this test. In order to achieve various performance measurements, several test scenarios are implemented as described in the subsections below.

**A. STEADY-STATE PERFORMANCE UNDER PSC**

The test model is examined in the presence of partial shading in a balanced grid, as well as a nonlinear loading scenario. The shadow is created with the help of a solar emulator. It caused multiple jumps in current on the voltage curve with respect to SPV, as well as the formation of several local maximum power points along the power curve of solar

photovoltaics. In the case of partial shading, the maximum solar photovoltaic voltage is 106.4 V and the maximum current is 15 A. Aside from that, the respective SPV has an efficiency rate of 99.78% in terms of available power, i.e., 1596 W, indicating that the majority of the energy is generated by the PV array. Fig. 8(a) depicts the grid currents injected to the grid from VSC while the DC-link voltage is held constant at its reference value derived from the global maximum power point. Fig. 8(b) depicts the phase voltage  $v_{sa}$ , grid current  $i_{sa}$ , compensation grid  $i_{ca}$ , load current  $i_{La}$  with respect to the grid. It can be observed that the compensation current of VSC system provides the nonlinear load requirements. Moreover, the grid current  $i_{sa}$  of SPV-DSTATCOM provides a sinusoidal current and maintains a unity power factor with respect to the grid voltage. Fig. 8(c) depicts the power flow for the entire system. It can be seen that the PV power  $p_{pv}$ , grid power  $p_g$ , and the load power  $p_L$  are 1.59kW, 1.1kW, and 565 W, respectively. Figs. 8(d), (e) and (f) show the percentage of THD for  $i_{sa}$ ,  $i_{ca}$  and  $i_{La}$ , respectively. It can be observed that % THD of  $i_{sa}$ ,  $i_{ca}$  and  $i_{La}$  are 1.68%, 9.74% and 26.24%, respectively. The THD of the injected grid current is maintained within 5% limit as per IEEE Standard 519-2014.

**B. TRANSIENT STATE PERFORMANCE WITH UNBALANCE LOADING UNDER PSC**

Figs. 9(a)-(c) show the dynamic performance of the SPV-DSTATCOM system when the b-phase load is perturbed.



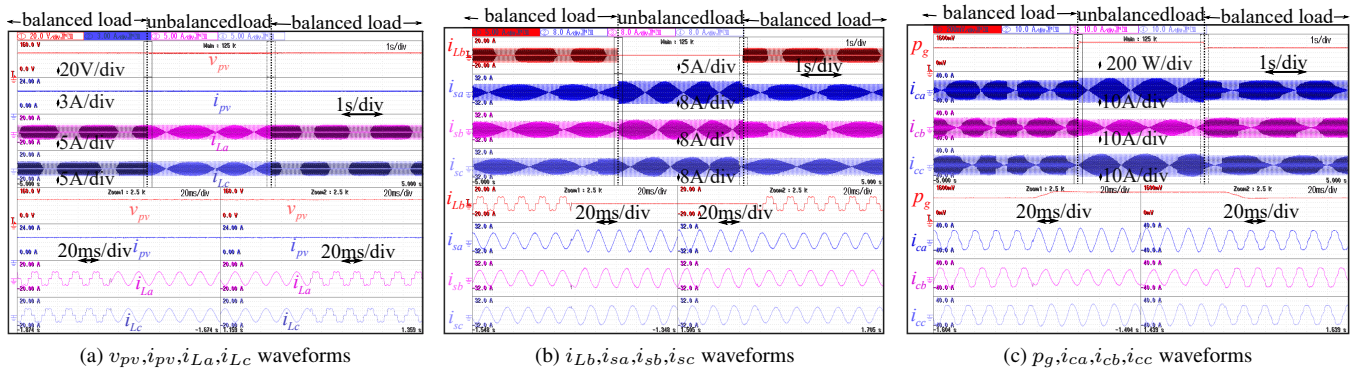


FIGURE 9. Experimental performance evaluation during load perturbation considering partial shading condition.

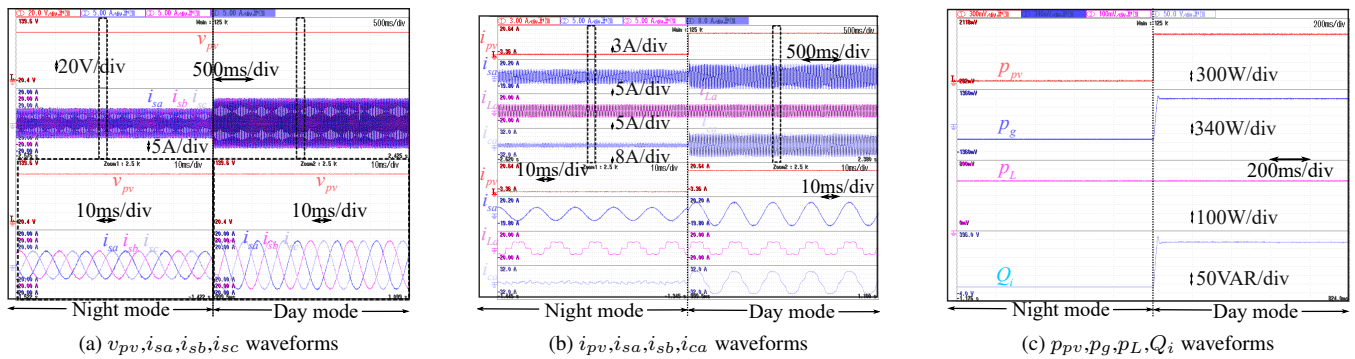


FIGURE 10. Experimental results: Dynamic condition analysis under PSC with changeover from night mode to day mode.

Because of the declination of the b-phase load, the net demand for harmonic current begins to decline. However, there is no change observed in PV current ( $I_{pv}$ ) and PV voltage ( $v_{pv}$ ), as observed in Fig. 9(a). Moreover,  $v_{pv}$  is maintained in accordance with the reference voltage generated by global MPPT. At the instant of removing the load, an increase in grid current ( $i_{sa}$ ,  $i_{sb}$ ,  $i_{sc}$ ) is observed in Fig. 9(b). As a result, the grid power increases, as illustrated in Fig. 9(c). The dynamics of VSC compensating currents ( $i_{ca}$ ,  $i_{cb}$ ,  $i_{cc}$ ) are shown in Fig. 9(c), where the VSC current of phase-b is observed to be sinusoidal as it does not have to supply harmonic current in phase-b.

### C. NIGHT MODE TO DAY MODE

The operating procedure of SPV-DSTATCOM from night to day is depicted in Fig. 10(a). Without solar radiation, the SPV-DSTATCOM system operates in the DSTATCOM mode using a 107 V DC-link voltage and a 0 A SPV current. In the presence of solar radiation, the SPV current increases from 0 A to 15 A while the DC-link voltage remains constant at 107 V, whereas the magnitude of the grid current begins to increase as shown in Fig. 10(b). The compensation current includes both the load current and the injected grid current during day mode. In Fig. 10(c), PV power  $P_{pv}$  is zero and maximum power during night and day mode conditions, respectively. The load power is constant during this scenario. The grid real power is negative during the night mode, which

indicates that grid power is delivered to the load and DC link capacitors. Here,  $Q_i$  indicates the reactive power injected by the DSTATCOM at the point of common coupling.

### D. SUDDEN CONNECTION OR DISCONNECTION OF THE NONLINEAR LOAD WITH SPV-DSTATCOM

The robustness of the proposed method is observed in SPV-DSTATCOM by instantaneous connection and disconnection of nonlinear load at constant solar irradiation, as shown in Fig. 11. At the sudden disconnection (connection) of the load, the grid current started increasing (decreasing) as shown in Fig. 11(a). Moreover, DC link voltage maintained constant as per the reference value of global MPPT during connecting or disconnecting the nonlinear load. It can be observed from Fig. 11(b) that the compensation current  $i_{ca}$  provides the load requirement during the loading condition. The current  $i_{ca}$  and  $i_{sa}$  are equal at no-load state. Moreover, The grid current and grid voltage are maintained in-phase considering unit power factor operation. The grid reactive power  $Q_g$  is nearly zero during connection or disconnection of the nonlinear load, as shown in Fig. 11(c). However, the PV power maintains constant during this period. The injected grid power reduces during loading, as the available PV power is constant at constant solar irradiance. During inductive loading only, the injected reactive power  $Q_i$  at PCC can be observed from Fig. 11(c).

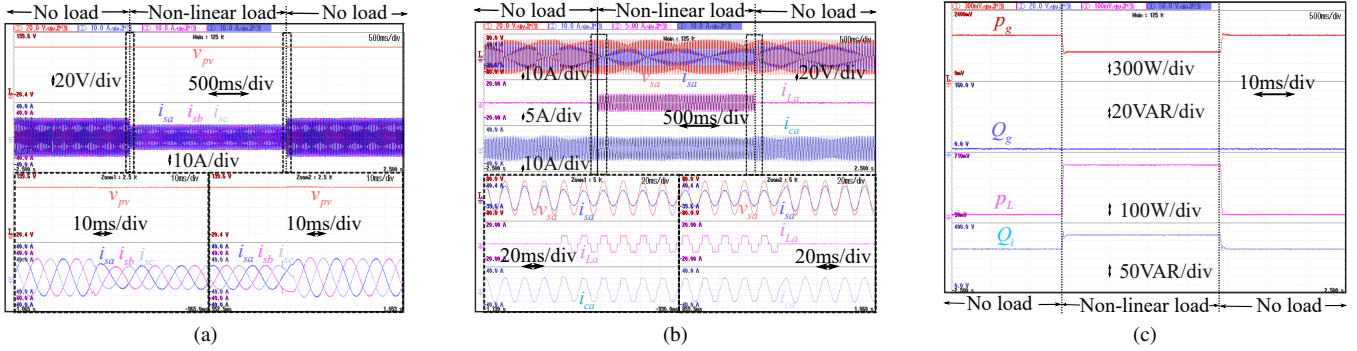


FIGURE 11. Dynamic condition analysis with PSC under sudden increment in load demand (a)  $v_{pu}, i_{sa}, i_{sb}, i_{sc}$  (b)  $v_{sa}, i_{sa}, i_{La}, i_{ca}$  (c)  $p_g, Q_g, P_L, Q_i$ .

TABLE 2. Comparative Analysis for proposed IPR-SOGI

Algorithm	Grid current THD	DC offset rejection	Steady state error	PSC	Computational complexity	DSP Speed	DC-link voltage ripple	Computation time	Requirement of cache memory
PR [36]	3.82%	no rejection	moderate	×	moderate	low	high	40 $\mu s$	high
DPR [37]	2.9%	less rejection capability	higher	×	comparatively higher	low	medium	50 $\mu s$	low
Proposed	3.1%	more rejection capability	lower	✓	lower	high	low	30 $\mu s$	low

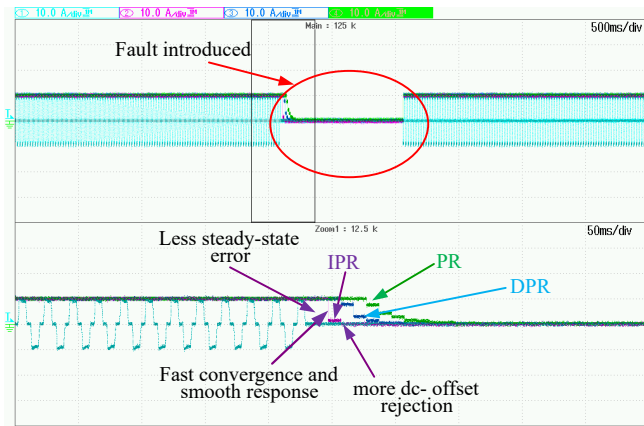


FIGURE 12. Dynamic response with Comparison performance of IPR-SOGI, PR and DPR

### E. COMPARISON RESULT

Fig. 12 depicts a comparative performance of the PR [36] and the damped PR (DPR) [37] based controllers with the proposed IPR-SOGI controller. This comparative study considers the performance indices such as dynamic response of weight components during load withdrawal. It can be observed from Fig. 12 that the suggested controller has a faster convergence time and lower steady-state error. Aside from that, IPR-SOGI has a higher dc-offset elimination capability.

Additionally, Table 2 is provided to indicate indices such as %THD, steady-state error, PSC, computational complexity, DC-link voltage fluctuation, and requirement of cache memory. It can be concluded that proposed IPR perform better during partial shading condition with lower computational burden.

### IV. CONCLUSION

The real-time execution of the grid-connected SPV-DSTATCOM system during partial shading conditions, with the goal of eliminating DC-offset, is demonstrated here. Through the use of the ESA, the accessible maximum power is generated from the SPV-DSTATCOM system with different transient scenarios. According to the findings of the preceding analysis for IPR-SOGI, the quality of power generated by the grid is improved by unpredictable SPV power generation accompanied by unusual grid and load scenarios. When compared with the traditional proportional resonance controller, the IPR-SOGI method yields excellent results in terms of DC-offset rejection and increased THD reduction potential, as well as increased system stability. Analytical investigations along with experimental validations are also performed in the laboratory for the SPV-DSTATCOM with the proposed IPR-SOGI controller. It is found that the grid current is injected with the desired power factor at less %THD than the permissible IEEE-519 limit.

## REFERENCES

- [1] W. Xiao, M. S. El Moursi, O. Khan, and D. Infield, "Review of grid-tied converter topologies used in photovoltaic systems," *IET Renewable Power Generation*, vol. 10, no. 10, pp. 1543–1551, 2016.
- [2] K. Wang, R. Zhu, C. Wei, F. Liu, X. Wu, and M. Liserre, "Cascaded multilevel converter topology for large-scale photovoltaic system with balanced operation," *IEEE Transactions on Industrial Electronics*, vol. 66, no. 10, pp. 7694–7705, 2019.
- [3] G. M. Madhu, C. Vyjayanthi, and C. N. Modi, "Investigation on effect of irradiance change in maximum power extraction from pv array interconnection schemes during partial shading conditions," *IEEE Access*, vol. 9, pp. 96 995–97 009, 2021.
- [4] S. K. Cherukuri, B. P. Kumar, K. R. Kaniganti, S. Muthubalaji, G. Devadasu, T. S. Babu, and H. H. Alhelou, "A novel array configuration technique for improving the power output of the partial shaded photovoltaic system," *IEEE Access*, vol. 10, pp. 15 056–15 067, 2022.
- [5] M. Kermadi, Z. Salam, A. M. Eltamaly, J. Ahmed, S. Mekhilef, C. Larbes, and E. M. Berkouk, "Recent developments of mppt techniques for pv systems under partial shading conditions: a critical review and performance evaluation," *IET Renewable Power Generation*, 2020.
- [6] H. Jeong, S. Park, J.-H. Jung, T. Kim, A.-R. Kim, and K. A. Kim, "Segmented differential power processing converter unit and control algorithm for photovoltaic systems," *IEEE Transactions on Power Electronics*, vol. 36, no. 7, pp. 7797–7809, 2020.
- [7] R. Motamarri and N. Bhookya, "Jaya algorithm based on lévy flight for global mppt under partial shading in photovoltaic system," *IEEE Journal of Emerging and Selected Topics in Power Electronics*, 2020.
- [8] N. Singh, K. K. Gupta, S. K. Jain, N. K. Dewangan, and P. Bhatnagar, "A flying squirrel search optimization for abb: Mppt under partial shaded photovoltaic system," *IEEE Journal of Emerging and Selected Topics in Power Electronics*, 2020.
- [9] A. Ostadrahimi and Y. Mahmoud, "Novel spline-mppt technique for photovoltaic systems under uniform irradiance and partial shading conditions," *IEEE Transactions on Sustainable Energy*, vol. 12, no. 1, pp. 524–532, 2020.
- [10] S. Rajendran and H. Srinivasan, "Simplified accelerated particle swarm optimisation algorithm for efficient maximum power point tracking in partially shaded photovoltaic systems," *IET Renewable Power Generation*, vol. 10, no. 9, pp. 1340–1347, 2016.
- [11] Y. Liu, J. Wei, X. Zong, W. Yi, and R. Liu, "Research on maximum power point tracking based on extremum seeking algorithm," in *2020 IEEE 4th Information Technology, Networking, Electronic and Automation Control Conference (ITNEC)*, vol. 1. IEEE, 2020, pp. 2502–2506.
- [12] N. Hui, D. Wang, and Y. Li, "A novel hybrid filter-based pll to eliminate effect of input harmonics and dc offset," *IEEE Access*, vol. 6, pp. 19 762–19 773, 2018.
- [13] R. Ma, J. Li, J. Kurths, S.-j. Cheng, and M. Zhan, "Generalized swing equation and transient synchronous stability with pll-based vsc," *IEEE Transactions on Energy Conversion*, pp. 1–1, 2021.
- [14] M. A. Awal and I. Husain, "Unified virtual oscillator control for grid-forming and grid-following converters," *IEEE Journal of Emerging and Selected Topics in Power Electronics*, vol. 9, no. 4, pp. 4573–4586, 2021.
- [15] M. Karimi-Ghartemani, S. A. Khajehoddin, P. K. Jain, A. Bakshshai, and M. Mojiri, "Addressing dc component in pll and notch filter algorithms," *IEEE Transactions on Power Electronics*, vol. 27, no. 1, pp. 78–86, 2011.
- [16] B. Shakerighadi, E. Ebrahimzadeh, M. G. Taul, F. Blaabjerg, and C. L. Bak, "Modeling and adaptive design of the srf-pll: Nonlinear time-varying framework," *IEEE Access*, vol. 8, pp. 28 635–28 645, 2020.
- [17] M. Mellouli, M. Hamouda, J. B. H. Slama, and K. Al-Haddad, "A third-order maf based qt1-pll that is robust against harmonically distorted grid voltage with frequency deviation," *IEEE Transactions on Energy Conversion*, vol. 36, no. 3, pp. 1600–1613, 2021.
- [18] A. Dash, D. P. Bagarty, P. K. Hota, R. K. Behera, U. R. Muduli, and K. Al Hosani, "Dc-offset compensation for three-phase grid-tied spv-dstatcom under partial shading condition with improved pr controller," *IEEE Access*, vol. 9, pp. 132 215–132 224, 2021.
- [19] A. Dash, D. P. Bagarty, P. K. Hota, U. R. Muduli, K. A. Hosani, and R. K. Behera, "Performance evaluation of three-phase grid-tied spv-dstatcom with dc-offset compensation under dynamic load condition," *IEEE Access*, vol. 9, pp. 161 395–161 406, 2021.
- [20] N. Mohammed and M. Ciobotaru, "Adaptive power control strategy for smart droop-based grid-connected inverters," *IEEE Transactions on Smart Grid*, pp. 1–1, 2022.
- [21] B. W. Franca, M. Aredes, L. F. d. Silva, G. F. Gontijo, T. C. Tricarico, and J. Posada, "An enhanced shunt active filter based on synchronverter concept," *IEEE Journal of Emerging and Selected Topics in Power Electronics*, vol. 10, no. 1, pp. 494–505, 2022.
- [22] J. C. Giacomini, L. Michels, H. Pinheiro, and C. Rech, "Active damping scheme for leakage current reduction in transformerless three-phase grid-connected pv inverters," *IEEE Transactions on Power Electronics*, vol. 33, no. 5, pp. 3988–3999, 2018.
- [23] D. Sun, X. Wang, H. Nian, and Z. Q. Zhu, "A sliding-mode direct power control strategy for dfig under both balanced and unbalanced grid conditions using extended active power," *IEEE Transactions on Power Electronics*, vol. 33, no. 2, pp. 1313–1322, 2018.
- [24] Y. Zou, L. Zhang, Y. Xing, Z. Zhang, H. Zhao, and H. Ge, "Generalized clarke transformation and enhanced dual-loop control scheme for three-phase pwm rectifiers under the unbalanced utility grid," *IEEE Transactions on Power Electronics*, pp. 1–1, 2022.
- [25] S. Dai, J. Wang, Z. Sun, and E. Chong, "Model inaccuracy analysis and compensation of stationary frame-based deadbeat predictive current control for high-speed pmsm drives," *IEEE Transactions on Transportation Electrification*, pp. 1–1, 2021.
- [26] G. C. Leandro, K. Sano, and N. Okada, "A variable admittance shunt capacitor using series inverter for filtering harmonics of distribution systems," *IEEE Journal of Emerging and Selected Topics in Power Electronics*, pp. 1–1, 2021.
- [27] J. S. Goud, R. Kalpana, B. Singh, and S. Kumar, "A global maximum power point tracking technique of partially shaded photovoltaic systems for constant voltage applications," *IEEE Transactions on Sustainable Energy*, vol. 10, no. 4, pp. 1950–1959, 2019.
- [28] N. Kumar, V. Saxena, B. Singh, and B. K. Panigrahi, "Intuitive control technique for grid connected partially shaded solar pv-based distributed generating system," *IET Renewable Power Generation*, vol. 14, no. 4, pp. 600–607, 2020.
- [29] A. K. Dubey, J. P. Mishra, and A. Kumar, "Modified ccf based shunt active power filter operation with dead-band elimination for effective harmonic and unbalance compensation in 3-phase 3-wire system," *IEEE Transactions on Power Delivery*, pp. 1–1, 2021.
- [30] S. Prakash, J. K. Singh, R. K. Behera, and A. Mondal, "A type-3 modified sogi-pll with grid disturbance rejection capability for single-phase grid-tied converters," *IEEE Transactions on Industry Applications*, vol. 57, no. 4, pp. 4242–4252, 2021.
- [31] P. Kanjiya, V. Khadkikar, and M. S. El Moursi, "Adaptive low-pass filter based dc offset removal technique for three-phase plls," *IEEE Transactions on Industrial Electronics*, vol. 65, no. 11, pp. 9025–9029, 2018.
- [32] I. E. Commission et al., "Photovoltaic (pv) systems-characteristics of the utility interface," *IEC Stand*, vol. 61727, 2004.
- [33] A. Dash, U. R. Muduli, S. Prakash, K. A. Hosani, S. R. Gongada, and R. K. Behera, "Modified proportionate affine projection algorithm based adaptive dstatcom control with increased convergence speed," *IEEE Access*, vol. 10, pp. 43 081–43 092, 2022.
- [34] H. A. Attia, T. K. S. Fredry, H. S. Che, W. P. Hew, and A. H. El Khateb, "Confined band variable switching frequency pulse width modulation (cbvsf pwm) for a single-phase inverter with an lcl filter," *IEEE Transactions on Power Electronics*, vol. 32, no. 11, pp. 8593–8605, 2017.
- [35] J. K. Singh, K. A. Jaafari, R. K. Behera, K. A. Hosani, and U. R. Muduli, "Faster convergence controller with distorted grid conditions for photovoltaic grid following inverter system," *IEEE Access*, vol. 10, pp. 29 834–29 845, 2022.
- [36] A. B. Acharya, D. Sera, L. E. Norum, and R. Teodorescu, "Frequency adaptive digital filter implementation of proportional-resonant controller for inverter applications," in *2018 IEEE 19th Workshop on Control and Modeling for Power Electronics (COMPEL)*. IEEE, 2018, pp. 1–7.
- [37] R. Chattopadhyay, A. De, and S. Bhattacharya, "Comparison of pr controller and damped pr controller for grid current control of lcl filter based grid-tied inverter under frequency variation and grid distortion," in *2014 IEEE Energy Conversion Congress and Exposition (ECCE)*. Ieee, 2014, pp. 3634–3641.





**BIBHUTI BHUSAN RATH** received B.E. and M.Tech. degree in Electrical Engineering from Utkal University, Bhubaneswar, India, in 1998 and Jawaharlal Nehru Technological University, Hyderabad, India, in 2011. He is currently working toward the Ph.D. degree in Electrical Engineering from Govind Ballabh Pant Institute of Engineering and Technology, Pauri Garhwal, Uttarakhand, India. His research includes the design of classical and intelligent controllers for solar photovoltaic

power systems and the application of soft computing methods in electric power systems.



**MANOJ KUMAR PANDA** (Senior Member, IEEE) received his B.E. and M.E. in Electrical Engineering and Control Instrumentation from Utkal University, India and Motilal Nehru National Institute of Technology Allahabad, India, in 1998 and 2002, respectively. He completed his Ph.D. in control system Engineering from Indian Institute of Technology Roorkee, India, in 2014. He is currently working as Professor in Electrical Engineering Department at Govind Ballabh Pant Institute of Engineering and Technology, Pauri Garhwal, Uttarakhand, India. He is an expert member of National Board of accreditation (NBA) wing of MHRD, Govt. of India. His areas of interest are in the field of soft computing and its engineering applications, renewable energy, and fuzzy control systems.



**BHOLA JHA** received B.Sc. and M.Tech. degree in Electrical Engineering and High Voltage Engineering from Muzaffarpur Institute of Technology, Muzaffarpur, Bihar, India and Jawaharlal Nehru Technological University, Hyderabad, India, in 1998 and 2004, respectively. He completed his Ph.D. in Electrical Engineering from Osmania University, Hyderabad, India, in 2013. Currently, He is working as an Associate Professor in the Department of Electrical Engineering of Govind

Ballabh Pant Institute of Engineering and Technology, Pauri Garhwal, Uttarakhand, India. His areas of research interests include the design of classical and intelligent controllers for solar photovoltaic power systems and the application of soft computing methods in electric power systems.



**AROBINDA DASH** (Graduate Student Member, IEEE) received the B.Tech. and M.Tech. in electrical engineering from Biju Patnaik University of Technology University, Odisha, India. He is pursuing his Ph.D. in electrical engineering from College of Engineering and Technology, Bhubaneswar, Odisha, India. His research interests include phase-locked loops, power electronics convertor and its application to power system, power system harmonics, renewable energy integration and grid synchronization.



**SURYA PRAKASH** (Graduate Student Member, IEEE) received B.Tech degree in electrical and electronics engineering from the JNTUH Hyderabad, India in 2009, and the M.Tech degree in power electronics engineering from VNIT Nagpur, Maharashtra in 2012. He is currently a Research Scholar with the Electrical Engineering Department, Indian Institute of Technology (IITP), Patna, Bihar, India. His research interest includes control methods for power electronics converters in distribution systems and renewable energy resources, grid interconnection issues, power quality enhancement, and low-voltage ride-through.



**RANJAN KUMAR BEHERA** (Senior Member, IEEE) received the B.Eng. Degree in electrical engineering from the Regional Engineering College (NIT) Rourkela, India, and the M. Tech. and Ph.D. degrees from the Indian Institute of Technology Kanpur, India, in 1998, 2003, and 2009, respectively. He has been a faculty member since 2009 and is currently an associate professor at the Department of Electrical Engineering, Indian Institute of Technology Patna, India. His research

interests include nonlinear control theory application to power electronic converters, pulse width modulation techniques and multiphase electric drives control.



**KHALIFA AL HOSANI** (Senior Member, IEEE) received the B.Sc. and M.Sc. degrees in electrical engineering from the University of Notre Dame, Notre Dame, IN, USA, in 2005 and 2007, respectively, and the Ph.D. degree in electrical and computer engineering from Ohio State University, Columbus, OH, USA, in 2011. He is currently an Associate Professor with the Department of Electrical and Computer Engineering, Khalifa University, Abu Dhabi, United Arab Emirates. He is the

CO-founder of the Power Electronics and Advanced Sustainable Energy Center Laboratory, ADNOC Research and Innovation Center, Abu Dhabi, United Arab Emirates. His research interests include a wide range of topics including nonlinear control, sliding mode control, control of power electronics, power systems stability and control, renewable energy systems modeling and control, smart grid, microgrid and distributed generation, and application of control theory to oil and gas applications.



**SRINIVASARAO TEGALA** (Member, IEEE) received his B.E. degree in Electrical and Electronics Engineering from Andhra University, India, M.E. degree in Power Systems Engineering from Jawaharlal Nehru Technological University, Hyderabad, and Ph.D. in Electrical Engineering from Andhra University, India, in 2000, 2007, and 2017, respectively. He is currently working as a Professor and head of the Department of Electrical and Electronics Engineering at Avanathi institute of

engineering and technology, Visakhapatnam, India. His areas of research include power system analysis, power system stability, renewable energy integration, microgrid, and high voltage engineering.



**UTKAL RANJAN MUDULI** (Member, IEEE) received the B.Tech. in electrical and electronics engineering from Biju Patnaik University of Technology Odisha, India, in 2011, and the M.Tech. in electrical engineering from the Indian Institute of Technology Gandhinagar, India, in 2014. He was a Visiting Scholar at the Department of Electrical Engineering and Computer Science, Khalifa University, UAE in 2019. He is currently pursuing his Ph.D. at the Indian Institute of Technology Patna,

India and working as research associate at Khalifa University, UAE. His research interests include modulation strategies for multiphase motor drives, matrix converters and its control, battery power management, and wireless power transfer.

...